

Temperature-Dependent Stability of Polytypes and Stacking Faults in SiC: Reconciling Theory and Experiments

Emilio Scalise[✉], Anna Marzegalli, Francesco Montalenti, and Leo Miglio

L-NESS and Department of Materials Science, University of Milano-Bicocca, Via Roberto Cozzi 55, 20125 Milan, Italy



(Received 6 March 2019; revised manuscript received 3 July 2019; published 29 August 2019)

The relative stability of SiC polytypes, changing with temperature, has been considered a paradox for about 30 years, due to discrepancies between theory and experiments. Based on *ab initio* calculations including van der Waals corrections, a temperature-dependent polytypic diagram consistent with the experimental observations is obtained. Results are easily interpreted based on the influence of the hexagonality on both cohesive energy and entropy. Temperature-dependent stability of stacking faults is also analyzed and found to be in agreement with experimental evidence. Our results suggest that lower temperatures during SiC crystal deposition are advantageous in order to reduce ubiquitous stacking faults in SiC-based power devices.

DOI: 10.1103/PhysRevApplied.12.021002

Silicon carbide has become the wide-band-gap (WBG) semiconductor with the most mature technology [1] and it is finally ready to penetrate the power devices market after more than two decades elapsed as a faint promise of next-generation power electronics [2,3]. Indeed, it is expected that SiC will reach about 10% of the Si market by 2025 with a compound annual growth rate (CAGR) of about 40% from 2020 to 2022 [4]. But, to continue the development of SiC technology and sustain the improvements in efficiency and performance of WBG-based devices, research efforts need to be continued even at the level of material physical understanding. In fact, the material maturity process has been quite slow. An evident reason is the intrinsic complexity of this semiconductor compound: it occurs only rarely in nature and it has more than 200 polytypes [5]. If properly understood and controlled, polytypism actually provides an added value. In fact, the most common SiC polytypes (3C-, 4H-, and 6H-SiC) cover a range of band gaps from about 2.3 to 3.2 eV and, thus, they are suitable both for low- and high-power devices.

Besides the scientific interest, investigating SiC polytypism and understanding its driving force is crucial to correctly predict the energetics of extended defects in SiC, particularly stacking faults (SFs), which are a main concern of this WBG semiconductor since they cause deterioration and eventually failure of the devices after a relatively long operational time [6–8].

SiC polytypes consist of identical double layers with different stacking sequences, thus generating orders of SiC tetrahedrons with different orientation, as highlighted in the blue and red colors in Fig. 1. Truly, SFs are wrong sequences of the double layers or, in other words, they can be seen as inclusions of a few layers of a SiC polytype in the perfect layer stacking of another polytype (see the inset

in Fig. 1). Because of the small-scale energy difference between the stacking sequences of double layers and hence between the different SiC polytypes, as discussed below, perturbations of the ideal stacking sequence during SiC crystal growth are very likely. This is another reason why SFs are so critical in this material.

The literature on the thermodynamic stability and polytypism of SiC is abundant, encouraged by the physical and technological interests evidenced above. Still, the predictions on the free energy of SiC polytypes are misleading and the energetic hierarchy reported by different theoretical methods is often inconsistent with some experimental observations. In fact, a paradox concerning SiC polytypes [10–13] has been often discussed, dealing with the theoretical predictions of the hexagonal (6H) SiC as the most stable polytype and of the cubic (3C) one as not stable at any temperature [11,14,15]. On the contrary, experiments have shown that the cubic (3C) structure does grow in preference to all others and only at very high temperatures have the hexagonal phases, i.e., 4H and 6H polytypes, been observed to prevail [10,14,16–20]. Thereby, SiC polytype stability at different temperatures remains unclear. Different arguments have been proposed over the years to explain polytypism and polytypic transformation in SiC [10,13,14,21–24], including the motion of partial dislocations [16,25–27] and impurity effects [10] on crystal growth. Nonetheless, inconsistencies between theory and experiments still remain.

Recently, it was shown that density-functional-theory (DFT) calculations including the van der Waals (vdW) correction do predict the 3C phase to have the lowest free energy at $T = 0$ K [28]. This intriguing result points out the importance of considering long-range interactions when comparing different SiC polytypes.

In this paper, we show that, by consistently adding the entropic contribution to the free energy, within a DFT

*emilio.scalise@unimib.it

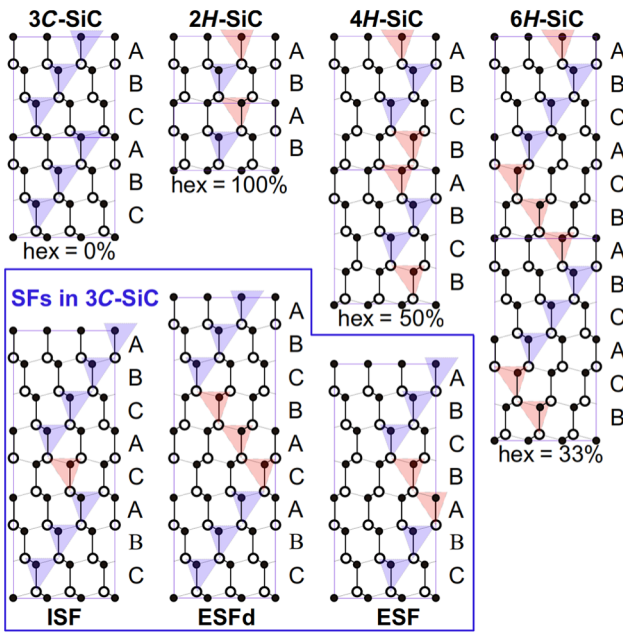


FIG. 1. Tetrahedral stacking sequences of 3C-, 2H-, 4H-, and 6H-SiC. The red and blue triangles highlight the twinned or normal tetrahedra and correspond to down or up spin configurations of the SiC layers, according to the axial next-nearest-neighbor Ising (ANNNI) model [9]. The inset shows the stacking sequence of the 3C-SiC polytype including an intrinsic, extrinsic, and double-extrinsic stacking fault (labeled ISF, ESF, and ESFd, respectively).

approach [29,30] that includes vdW corrections, the full T -dependent hierarchy of polytypes is correctly predicted, showing a crossover between 3C and 6H (or 4H) phases at typical experimental temperatures. This allows one to understand the physics behind SiC polytypism by simple

thermodynamics considerations, highlighting the correlation among hexagonality, vibrational properties, and cohesive energy. Moreover, calculations of the stability of SiC SFs reveal a T -dependent behavior, intimately correlated to the polytypic stability, and they provide insight into the optimal growth temperatures for lowering the density of such defects. The results shown here point to a general trend in the physical aspects governing the polytype stability, which may be extended to other semiconductors, such as zinc chalcogenides, and may also be exploited to rationalize aspects of transformations observed in GaN [31] or InP [32].

In Table I, the lattice constants of 3C-, 6H-, 4H-, and 2H-SiC are reported, both calculated at the generalized-gradient approximation (GGA) level [33] and with the semiempirical Grimme's method, which employs GGA-type density functionals constructed with a long-range dispersion correction [34,35] and accounting for vdW interactions. It is evident that the agreement between theoretical and experimental lattice parameters improves considerably for vdW-corrected DFT simulations. These improvements are even more appreciable by looking at the heat of formation (ΔH_f) in Table I, which is severely underestimated by GGA but in very good agreement with experiments in the case of vdW-corrected simulations. Note that not only the magnitude of the heat of formation but also the order of the values calculated for the different polytypes changes whether or not the simulations include the vdW correction. This is very clear looking at the total energy of the different polytypes (ΔE_T) in Table I, calculated as a relative value with respect to the total energy of 3C-SiC. While ΔE_T values calculated by GGA are all negative except for 2H-SiC, thus predicting 3C-SiC as the least stable polytype after the 2H-SiC, the vdW-corrected

TABLE I. Percentage hexagonality (Hex.) of the SiC structures, their lattice constants (a for the cubic cell, a and c for the hexagonal ones, in Å), total energy ΔE_T (relative to 3C-SiC) and heat of formation ΔH_f (meV/SiC) of 3C-, 6H-, 4H- and 2H-SiC. Value are calculated at the GGA level without or with vdW correction. Experimental values (Expt.) are also reported, but blank spaces indicating that no corresponding data has been found.

Polytype	Hex.	a, c	ΔE_T	ΔH_f
3C-SiC	0%			
GGA		4.377	0	-402
GGA(vdW)		4.352	0	-785
Expt. [36–39]		4.3596		-650, -758, -771
6H-SiC	33%			
GGA		3.093, 15.178	-1.7	-404
GGA(vdW)		3.075, 15.105	1.4	-784
Expt. [36–38,40]		3.080, 15.117		-676, -747, -771
4H-SiC	50%			
GGA		3.092, 10.123	-1.8	-404
GGA(vdW)		3.074, 10.079	2.9	-783
Expt. [39–41]		3.073, 10.053		-650, -689
2H-SiC	100%			
GGA		3.090, 5.072	5.8	-396
GGA(vdW)		3.072, 5.056	15.1	-770
Expt. [42]		3.079, 5.053		

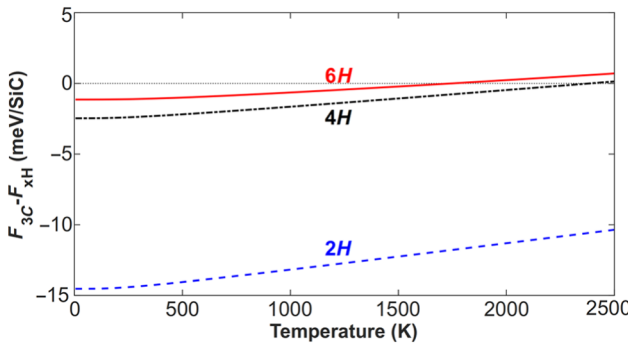


FIG. 2. Difference between the Helmholtz free energy of 3C-SiC with respect to the value of 6H, 4H, and 2H polytypes.

simulations give all positive ΔE_T . Hence, 3C-SiC turns out to be the most stable polytype. This is in good agreement with both experimental evidence inferring 3C-SiC as the most stable SiC structure in the nuclear stage [40] and a recent theoretical work [28]. Nevertheless, the predicted energetic hierarchy at $T = 0$ K is still not sufficient to understand the competition in stability of SiC polytypes at higher temperature, as probed experimentally [16–20,27]. Thus, the variation of the entropic contributions with temperature for the different polytypes becomes crucial. This has been included in Fig. 2, where the Helmholtz free energy for the SiC polytypes is plotted as a difference between the values of the 2H, 4H, and 6H polytypes and that of 3C-SiC.

The typical expression of the Helmholtz free energy $F(T) = U - TS$, with U the internal energy and TS the product of temperature and entropy, can also be reformulated as $F(T) = U_0 + U_{\text{vib}} - TS$, where the internal energy U is split into the vibrational internal energy (U_{vib}) and static internal energy (U_0), with the latter corresponding to the total DFT energy of the SiC polytypes at their GGA vdW equilibrium geometry. Also, the other terms of the Helmholtz free energy can be conveniently calculated by DFT [43]. In fact, one can additionally formulate $F(T)$ as a sum of the electronic and vibrational contributions, thus $F(T) = F_{\text{el}}(T) + F_{\text{vib}}(T)$. The former term $F_{\text{el}}(T)$ can be reasonably approximated by its zero-temperature limit (U_0) [14], by neglecting the electronic entropy; the vibrational contribution, which then corresponds to $F_{\text{vib}}(T) = U_{\text{vib}} - TS$, can be calculated by the quasiharmonic approximation as [15,44]

$$F_{\text{vib}}(T) = \int_0^\infty g(\omega) \left[\frac{\hbar\omega}{2k_B T} + \ln(1 - e^{-\hbar\omega/k_B T}) \right] d\omega,$$

where ω is the phonon frequency and $g(\omega)$ is the phonon density of states. In our simulations, ω and $g(\omega)$ are calculated in the framework of the density-functional perturbation theory (DFPT) [43,45].

The values at $T = 0$ K of the three curves plotted in Fig. 2 reveal that the zero-point internal energy (ZPE),

which is the main contribution to F_{vib} in the low-temperature range, only slightly affects the static internal energy (cf. ΔE_T in Table I) and does not change the energetic hierarchy of the SiC polytypes. But for temperatures above 500 K, the vibrational contribution (F_{vib}) becomes considerable and the Helmholtz free energies of the hexagonal polytypes get closer to the cubic one. Particularly, at temperatures of about 1750 K, the difference between the free energies ($F_{3C} - F_{6H}$) crosses the 0 energy line, meaning that the 6H polytype becomes thermodynamically more stable than 3C. The energy crossing between 4H- and 3C-SiC is predicted a bit higher in temperature, at about 2400 K. On the contrary, 2H never becomes more stable than 3C-SiC in the temperature range considered, albeit their free energies get closer at higher temperatures. The comparison between hexagonal polytypes reveals that 2H-SiC is the least thermodynamically stable structure: the difference of its free energy and that of the 4H or 6H polytype marginally decreases with the temperature. On the contrary, the free energies of the 6H and 4H polytypes get very close at temperatures around 2500 K. Our T -dependent diagram of the polytypic stability plotted in Fig. 2 is in excellent agreement with several pieces of experimental evidence such as the preferential growth at temperatures below approximately 1850 K of the 3C polytype over all others [10,14,21], the higher stability of the 4H and 6H polytypes at higher temperatures [16–20,27], and the rare appearance of 2H-SiC [26,46].

The correlation between hexagonality and the observed trends in the Helmholtz free energy is elucidated by the calculated entropy, $S = -(\delta F_{\text{vib}}/\delta T)$, reported in Fig. 3. An opposite hierarchy of the entropy with respect to the cohesive energy at all temperatures is found. This is further supported by the general decreasing trend of phonon frequencies with hexagonality, which is evident in the phonon density of states (PDOS) plotted for the different polytypes in the region of the longitudinal optical (LO) branch [47] in the inset of Fig. 3. The shift of the phonon frequencies is associated to a different strength of the interactions between hexagonally and cubically stacked layers; thus, a correspondence between the lower

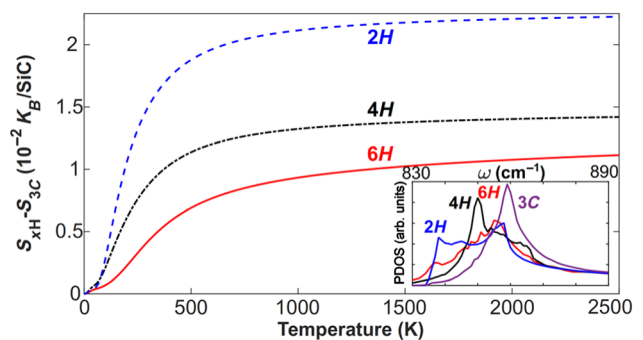


FIG. 3. Difference between the entropy of xH and 3C polytypes. The inset shows the PDOS in the region near the LO band.

hexagonality and the higher cohesion of the structure is evident. The difference in the free energy at $T = 0$ K between 3C- and 2H-SiC is so large compared to their entropy difference that 2H remains less stable even at high temperature. On the contrary, the much smaller difference between the static energy of 3C and 6H (or 4H) is overcompensated by the larger entropy contribution of the latter.

These conclusions provide an intuitive picture to understand SiC polytypism and identify a general trend in the physical aspects responsible for polytypism, elucidating the relation between structural properties (crystal symmetry and cohesive energy) and relative stability in temperature: the crystal hierarchy, from stiffer to softer phase, determines a decreasing trend in stability at $T = 0$ K, but an increasing trend in the vibrational entropy, eventually producing a crossover in the free energy. The observed temperature-driven polytype change in zinc chalcogenides [48–51], for instance, can be perfectly understood within this interpretative scheme [47].

The correct prediction of the free energy of polytypes is a compelling need for the investigation of other essential aspects of SiC and it is exploited below to study the SF stability. The energetic cost of any error in the stacking sequence can be estimated by two different approaches: modeling a perturbed layer stacking by supercell structures, such as those illustrated in the inset of Fig. 1, and then calculating the total energy of the faulted supercell, or alternatively calculating the SF energy according to the ANNNI model [9,52]. In fact, the energy of the different polytypes, both pristine or faulted, can be expressed in terms of the interactions between SiC double layers. Accordingly, for the xH - (or xC -) SiC polytypes, the total free energy is

$$E = E_0 - \frac{1}{x} \sum_{i=1}^n \sum_{j=1}^{\infty} J_j \sigma_i \sigma_{i+j}, \quad (1)$$

where E_0 is a common reference energy and J_j are the interaction energies between i th-neighbor double layers. The double layers are represented by a pseudospin σ_i , which can be spin-up or spin-down (with value +1 or -1,

respectively) according to the tetrahedron orientation that the layers form: $\sigma_i = +1$ corresponds to a normal orientation (blue in Fig. 1) while $\sigma_i = -1$ to a twinned one (red in Fig. 1) [21,25]. For instance, 4H-SiC is represented by two spin-up and two spin-down and 6H by three up and three down. In Eq. (1), spin couplings higher than third order are usually neglected. The static free energies of Table I can then be used to obtain the J_j values from Eq. (1), and they allow one to calculate the free energies of faulted structures. Finally, stacking fault energies are estimated as the energy difference between the faulted and the pristine structure [24,27,53] and they are listed in Table II. We also checked the reliability of the SF energies calculated by the ANNNI model, comparing them with the corresponding value obtained by simulating the defected supercells of 3C-SiC, as illustrated in the inset of Fig. 1. Interestingly, the calculated SF energy values are all positive and in excellent agreement with experimental estimations [53,56] if the vdW correction is included in the DFT simulations. In contrast, SF energies obtained by bare GGA are very different, particularly for 3C-SiC. In fact, the formation energy of intrinsic stacking faults (ISFs) in 3C-SiC calculated by GGA is much lower than the corresponding value obtained including the vdW correction. For extrinsic stacking faults, both single (ESF) and double (ESFd), the SF energies even turn into negative values. This is not surprising if one goes through the literature of SFs in 3C-SiC, in which very small or even negative theoretical values of the ESF energy in 3C-SiC are well accepted (see Table II). Instead, these SF energies are doubtful if compared with experiments [56]. Typically, SF energy is experimentally estimated by comparing the measured width of the stacking fault between the two terminating partial dislocations [53,56] and its expectation by means of the dislocation theory for anisotropic elastic media [53,56,57]. Accordingly, SFs with negative formation energies should not have finite width and thus are in evident contradiction with experiments.

Finally, by exploiting the T -dependent free energies presented above, we plot in Fig. 4 the SF formation energies for the 3C-, 6H-, and 4H-SiC as a function of the temperature. Particularly, by using each value of the Helmholtz

TABLE II. Formation energy (mJ m^{-2}) of SFs in 3C-, 6H-, and 4H-SiC. Experimental values (Expt.) from [53,56] and other theoretically calculated (Calc.) values from [24,54,55] are also listed.

	3C-SiC			6H-SiC	4H-SiC
	ISF	ESF	ESFd	ISF	ISF
GGA	4.35	-16.7	-19.5	2.84	18.23
GGA vdW	40.70	19.6	16.85	2.77	18.35
Supercell	40.21	19.62	17.04		
Expt.	34			2.9 ± 0.6	14.7 ± 2.5
Calc. [24]	-6.27			3.14	18.3
Calc. [54]	10.3	-7.83	-11.6		
Calc. [55]	-3.4	-28			

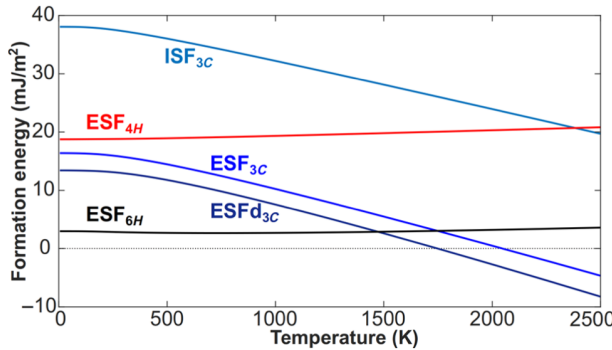


FIG. 4. Formation energy of ISF in 6H- and 4H-SiC and of ISF, ESF, and ESFd in 3C-SiC.

free energies, which include the entropy at different temperatures as plotted in Fig. 2, the parameters in the ANNNI model and then the SF energies are calculated for any corresponding temperature. Different trends in temperature between hexagonal and cubic polytypes are found: while the formation energies of SF in 6H- and 4H-SiC slightly increase with the temperature, for 3C-SiC the SF energies decrease substantially with the temperature and, particularly for the ESFs, they become negative at temperatures above 1750 K.

In conclusion, we show that DFT calculations including the vdW correction predict a T -dependent hierarchy of SiC polytypes in perfect agreement with the experimental results. 3C-SiC is predicted to have the highest cohesive energy but the lowest entropy. At high temperature, the higher entropic contribution to the free energy of the hexagonal polytypes stabilizes their structures, with the 6H- and 4H-SiC becoming thermodynamically more stable than 3C-SiC. These results demonstrate the key role of the thermodynamics in determining SiC polytypism and contribute to finally reconciling theory and experiments. They also evidence a general trend in the physical aspects governing the polytype stability, which may be extended to other semiconductors, such as zinc chalcogenides. Based on this understanding, an accurate analysis of SF stability in SiC is also performed, revealing positive formation-energy values for both ESF and ISF in 3C-SiC that decrease substantially with temperature, becoming lower than that predicted for 6H-SiC and eventually negative. Importantly, this indicates that too-high deposition temperatures should be avoided in order to decrease SF density in 3C-SiC.

Acknowledgments The authors acknowledge the EU for founding the CHALLENGE project (3C-SiC Hetero-Epitaxially Grown on Silicon Compliance Substrates and 3C-SiC Substrates for Sustainable Wide-Band-Gap Power Devices) within the EU's H2020 Industrial Leadership framework program for research and innovation under Grant No. 720827. The CINECA award under the ISCRA initiative, for the availability of high-performance computing resources and support, is also acknowledged.

- [1] T. Kimoto, Material science and device physics in SiC technology for high-voltage power devices of thermal oxidation and hydrogen annealing, *Jpn. J. Appl. Phys.* **54**, 040103 (2015).
- [2] V. E. Chelnokov, A. L. Syrkin, and V. A. Dmitriev, Overview of SiC power electronics, *Diam. Relat. Mater.* **6**, 1480 (1997).
- [3] M. Willander, M. Friesel, Q. U. Wahab, and B. Straumal, Silicon carbide and diamond for high temperature device applications, *J. Mater. Sci. Mater. Electron.* **17**, 1 (2006).
- [4] A. Bhalla, in *Disruptive Wide Bandgap Semiconductors, Related Technologies, and Their Applications* (InTech, 2018).
- [5] N. W. Jepps and T. F. Page, Polytypic transformations in silicon carbide, *Prog. Cryst. Growth Charact.* **7**, 259 (1983).
- [6] Y. Ishida, M. Kushibe, T. Takahashi, H. Okumura, and S. Yoshida, Investigation of the relationship between defects and electrical properties of 3C-SiC epilayers, *Mater. Sci. Forum* **389-393**, 459 (2002).
- [7] H. Nagasawa, M. Abe, K. Yagi, T. Kawahara, and N. Hatta, Fabrication of high performance 3C-SiC vertical MOSFETs by reducing planar defects, *Phys. Status Solidi B Basic Res.* **245**, 1272 (2008).
- [8] J. Eriksson, F. Roccaforte, M. H. Weng, F. Giannazzo, J. Lorenzzi, and V. Raineri, Electrical activity of structural defects in 3C-SiC, *Mater. Sci. Forum* **679-680**, 273 (2011).
- [9] M. E. Fisher and W. Selke, Infinitely Many Commensurate Phases in a Simple Ising Model, *Phys. Rev. Lett.* **44**, 1502 (1980).
- [10] V. Heine, C. Cheng, and R. J. Needs, The preference of silicon carbide for growth in the metastable cubic form, *J. Am. Ceram. Soc.* **74**, 2630 (1991).
- [11] C. Cheng, V. Heine, and R. J. Needs, Atomic relaxation in silicon carbide polytypes, *J. Phys. Condens. Matter* **2**, 5115 (1990).
- [12] J. Fan and P. K. Chu, *Silicon Carbide Nanostructures, Engineering Materials and Processes* (Springer International Publishing, Cham, 2014).
- [13] A. Zywieltz, K. Karch, and F. Bechstedt, Influence of polytypism on thermal properties of silicon carbide, *Phys. Rev. B Condens. Matter Mater. Phys.* **54**, 1791 (1996).
- [14] F. Bechstedt, P. Käckell, A. Zywieltz, K. Karch, B. Adolph, K. Tenelsen, and J. Furthmüller, Polytypism and properties of silicon carbide, *Phys. Status Solidi (b)* **202**, 35 (1997).
- [15] Z. C. Feng, *SiC Power Materials: Devices and Applications* (Springer, 2004), p. 450.
- [16] A. Boulle, D. Dompoint, I. Galben-Sandulache, and D. Chaussende, Quantitative analysis of diffuse X-ray scattering in partially transformed 3C-SiC single crystals, *J. Appl. Crystallogr.* **43**, 867 (2010).
- [17] M. Kanaya, J. Takahashi, Y. Fujiwara, and A. Moritani, Controlled sublimation growth of single crystalline 4H-SiC and 6H-SiC and identification of polytypes by x-ray diffraction, *Appl. Phys. Lett.* **58**, 56 (1991).
- [18] R. Yakimova, M. Syväjärvi, T. Iakimov, H. Jacobsson, R. Rback, A. Vehanen, and E. Janzén, Polytype stability in seeded sublimation growth of 4H-SiC boules, *J. Cryst. Growth* **217**, 255 (2000).

- [19] K. Motohisa, D. Hironori, S. Hidemitsu, S. Hiroshi, B. Takeshi, Y. Nobuyoshi, K. Kazuhiko, O. Nobuhiro, M. Kouji, and K. Kazuhito, High-speed growth of 4H-SiC single crystal using Si–Cr based melt, *Mater. Sci. Forum* **740-742**, 73 (2013).
- [20] K. Kusunoki, N. Okada, K. Kamei, K. Moriguchi, H. Daikoku, M. Kado, H. Sakamoto, T. Bessho, and T. Ujihara, Top-seeded solution growth of three-inch-diameter 4H-SiC using convection control technique, *J. Cryst. Growth.* **395**, 68 (2014).
- [21] C. Cheng, R. J. Needs, and V. Heine, Inter-layer interactions and the origin of SiC polytypes, *J. Phys. C: Solid State Phys.* **21**, 1049 (1988).
- [22] W. Y. Ching, Y. N. Xu, P. Rulis, and L. Ouyang, The electronic structure and spectroscopic properties of 3C, 2H, 4H, 6H, 15R and 21R polymorphs of SiC, *Mater. Sci. Eng. A* **422**, 147 (2006).
- [23] N. Bernstein, H. J. Gotsis, D. A. Papaconstantopoulos, and M. J. Mehl, Tight-binding calculations of the band structure and total energies of the various polytypes of silicon carbide, *Phys. Rev. B Condens. Matter Mater. Phys.* **71**, 1 (2005).
- [24] U. Lindefelt, H. Iwata, S. Öberg, and P. R. Briddon, Stacking faults in SiC, *Phys. Rev. B* **67**, 155204 (2003).
- [25] P. Pirouz and J. W. Yang, Polytypic transformations in SiC: The role of TEM, *Ultramicroscopy* **51**, 189 (1993).
- [26] P. Pirouz, Polytypic transformations in SiC, *Solid State Phenom.* **56**, 107 (1997).
- [27] A. Boulle, D. Dompoint, I. Galben-Sandulache, and D. Chaussende, Polytypic transformations in SiC: Diffuse x-ray scattering and Monte Carlo simulations, *Phys. Rev. B* **88**, 024103 (2013).
- [28] S. Kawanishi and T. Mizoguchi, Effect of van der Waals interactions on the stability of SiC polytypes, *J. Appl. Phys.* **119**, 175101 (2016).
- [29] P. Giannozzi, *et al.*, QUANTUM ESPRESSO: A modular and open-source software project for quantum simulations of materials, *J. Phys. Condens. Matter* **21**, 395502 (2009).
- [30] P. E. Blochl, Projector augmented-wave method, *Phys. Rev. B* **50**, 24 (1994).
- [31] W. Y. Pang, I. Lo, S. Wu, Z. X. Lin, C. H. Shih, Y. C. Lin, Y. C. Wang, C. H. Hu, and G. Z. L. Hsu, Growth of Wurtzite and Zinc-Blende phased GaN on silicon (100) substrate with sputtered AlN buffer layer, *J. Cryst. Growth.* **382**, 1 (2013).
- [32] P. Staudinger, S. Mauthe, K. E. Moselund, and H. Schmid, Concurrent Zinc-Blende and Wurtzite film formation by selection of confined growth planes, *Nano Lett.* **18**, 7856 (2018).
- [33] J. P. Perdew, K. Burke, and M. Ernzerhof, Generalized Gradient Approximation Made Simple, *Phys. Rev. Lett.* **77**, 3865 (1996).
- [34] V. Barone, M. Casarin, D. Forrer, M. Pavone, M. Sambi, and A. Vittadini, Role and effective treatment of dispersive forces in materials: Polyethylene and graphite crystals as test cases, *J. Comput. Chem.* **30**, 934 (2009).
- [35] S. Grimme, Semiempirical GGA-type density functional constructed with a long-range dispersion correction, *J. Comput. Chem.* **27**, 1787 (2006).
- [36] J. R. O'Connor and J. Smiltens, *Silicon Carbide, a High Temperature Semiconductor: Proceedings* (Symposium Publications Division, Pergamon Press, 1960).
- [37] H. Kleykamp, Gibbs energy of formation of SiC: A contribution to the thermodynamic stability of the modifications, *Berichte der Bunsengesellschaft für physikalische Chemie* **102**, 1231 (1998).
- [38] E. Greenberg, C. A. Natke, and W. N. Hubbard, The enthalpy of formation of silicon carbide by fluorine bomb calorimetry, *J. Chem. Thermodyn.* **2**, 193 (1970).
- [39] W. M. Haynes, ed., *CRC Handbook of Chemistry, Physics: A Ready-reference Book of Chemical and Physical Data* (CRC Press, Boca Raton, 2014), 95th ed.
- [40] Y. M. Tairov and V. F. Tsvetkov, Progress in controlling the growth of polytypic crystals, *Progress in Crystal Growth and Characterization* **7**, 111 (1983).
- [41] J. Zemann, Crystal structures, 2nd edition. Vol. 1 by R. W. G. Wyckoff, *Acta Crystallogr.* **18**, 139 (1965).
- [42] H. Schulz and K. H. Thiemann, Structure parameters and polarity of the Wurtzite type compounds SiC-2H AND ZnO, *Solid State Commun.* **32**, 783 (1979).
- [43] S. Baroni, P. Giannozzi, and E. Isaev, Density-functional perturbation theory for quasi-harmonic calculations, *Rev. Mineral. Geochem.* **71**, 39 (2010).
- [44] M. Born, K. Huang, and M. Lax, Dynamical theory of crystal lattices, *Am. J. Phys.* **23**, 474 (1955).
- [45] S. Baroni, P. Giannozzi, and A. Testa, Greens-function Approach to Linear Response in Solids, *Phys. Rev. Lett.* **58**, 1861 (1987).
- [46] M. Imade, T. Ogura, M. Uemura, F. Kawamura, M. Yoshimura, Y. Kitaoka, T. Sasaki, Y. Mori, M. Yamazaki, S. Suwabe, and S. Nakashima, Liquid-phase epitaxy of 2H-SiC film on a (0001) 4H-SiC substrate in Li-Si melt, *Mater. Lett.* **63**, 649 (2009).
- [47] See the <http://link.aps.org/supplemental/10.1103/PhysRevApplied.12.021002> for details on the theoretical method and for the complete PDOS plot.
- [48] C.-Y. Yeh, Z. W. Lu, S. Froyen, and A. Zunger, Zinc-Blende-Wurtzite polytypism in semiconductors, *Phys. Rev. B* **46**, 10086 (1992).
- [49] R. R. Reeber, The correspondence of lattice characteristic temperatures with Debye temperatures of some inorganic compounds, *Phys. Status Solidi (a)* **26**, 253 (1974).
- [50] J. A. Birch, Heat capacities of ZnS, ZnSe and CdTe below 25 K, *J. Phys. C: Solid State Phys.* **8**, 2043 (1975).
- [51] J. Baars and G. Brandt, Structural phase transitions in ZnS, *J. Phys. Chem. Solids* **34**, 905 (1973).
- [52] S. Limpijumnong and W. R. L. Lambrecht, Total energy differences between SiC polytypes revisited, *Phys. Rev. B Condens. Matter Mater. Phys.* **57**, 12017 (1998).
- [53] M. H. Hong, A. V. Samant, and P. Pirouz, Stacking fault energy of 6H-SiC and 4H-SiC single crystals, *Philos. Mag. A* **80**, 919 (2000).
- [54] Y. Umeno, K. Yagi, and H. Nagasawa, Ab initio density functional theory calculation of stacking fault energy and stress in 3C-SiC, *Phys. Status Solidi (b)* **249**, 1229 (2012).
- [55] P. Käckell, J. Furthmüller, and F. Bechstedt, Stacking faults in group-IV crystals: An ab initio study, *Phys. Rev. B Condens. Matter Mater. Phys.* **58**, 1326 (1998).
- [56] X. G. Ning and H. Q. Ye, Experimental determination of the 8 intrinsic stacking-fault energy of SiC crystals, *J. Phys. Condens. Matter* **2**, 10223 (1990).
- [57] P. J. Hirth and J. Lothe, *Theory of Dislocations* (Wiley, New York, 1982).